Available online at www.sciencedirect.com
ScienceDirect
Journal of Structural Biology 159 (2007) 9–18
Journal of Structural Biology
www.elsevier.com/locate/yjsbi

Octomeric pyruvate-ferredoxin oxidoreductase from *Desulfovibrio vulgaris*

Florian Garczarek [a], Ming Dong [a], Dieter Typke [a], H. Ewa Witkowska [b], Terry C. Hazen [c], Eva Nogales [a,d,*], Mark D. Biggin [a,*], Robert M. Glaeser [a,*]

[a] *Life Sciences Division, Lawrence Berkeley National Laboratory, University of California, Berkeley, CA 94720, USA*
[b] *UCSF Biomolecular Resource Center Mass Spectrometry Facility and Department of Cell and Tissue Biology, University of California, San Francisco, CA 94143, USA*
[c] *Earth Sciences Division, Lawrence Berkeley National Laboratory, University of California, Berkeley, CA 94720, USA*
[d] *Howard Hughes Medical Institute, Department of Molecular and Cell Biology, University of California, Berkeley, CA 94720, USA*

Received 13 December 2006; received in revised form 17 January 2007; accepted 19 January 2007
Available online 17 February 2007

Abstract

Pyruvate-ferredoxin oxidoreductatse (PFOR) carries out the central step in oxidative decarboxylation of pyruvate to acetyl-CoA. We have purified this enzyme from *Desulfovibrio vulgaris* Hildenborough (*Dv*H) as part of a systematic characterization of as many multi-protein complexes as possible for this organism, and the three-dimensional structure of this enzyme has been determined by a combination of electron microscopy (EM), single particle image analysis, homology modeling and computational molecular docking. Our results show that the 1 MDa *Dv*H PFOR complex is a homo-octomer, or more precisely, a tetramer of the dimeric form of the related enzyme found in *Desulfovibrio africanus* (*Da*), with which it shares a sequence identity of 69%. Our homology model of the *Dv*H PFOR dimer is based on the *Da* PFOR X-ray structure. Docking of this model into our 17 Å resolution EM-reconstruction of negatively stained *Dv*H PFOR octomers strongly suggests that the difference in oligomerization state for the two species is due to the insertion of a single valine residue (Val383) within a surface loop of the *Dv*H enzyme. This study demonstrates that the strategy of intermediate resolution EM reconstruction coupled to homology modeling and docking can be powerful enough to infer the functionality of single amino acid residues.

Keywords: Pyruvate-ferredoxin oxidoreductase; *Desulfovibrio vulgaris*; Electron microscopy; Single particle reconstruction; Oligomerization; Homology modeling; Molecular docking

1. Introduction

The oxidative decarboxylation of pyruvate to produce acetyl-CoA is the gateway to the tricarboxylic acid (TCA) cycle. In aerobic bacteria, this central step in energy metabolism is catalyzed by the pyruvate dehydrogenase multi-enzyme complex. In most anaerobic bacteria, archaea, and eukaryotes that lack mitochondria, however, this step is catalyzed by the enzyme pyruvate-ferredoxin oxidoreductase (PFOR) (Charon et al., 1999).

The subunit composition of PFOR varies in different organisms. In some species PFOR occurs as a dimer of a single polypeptide (Brostedt and Nordlund, 1991). In others, four or five different genes encode smaller polypeptides that assemble to form the functional PFOR (Brostedt and Nordlund, 1991; Ikeda et al., 2006). These genes are homologous to different parts of the larger single-polypeptide PFORs, and it is thought that the single polypeptide PFORs arose by operon rearrangement and fusion of smaller common ancestor genes (Kletzin and Adams, 1996).

* Corresponding authors. Address: Howard Hughes Medical Institute, Department of Molecular and Cell Biology, University of California, Berkeley, CA 94720, USA. Fax: +1 510 486 6488.
E-mail addresses: enogales@lbl.gov (E. Nogales), mdbiggin@lbl.gov (M.D. Biggin), rmglaeser@lbl.gov (R.M. Glaeser).

1047-8477/$ - see front matter © 2007 Elsevier Inc. All rights reserved.
doi:10.1016/j.jsb.2007.01.020

Previously, the only structure reported for a PFOR was the X-ray crystal structure of a 266 kDa homodimeric enzyme from the sulfate reducing bacterium *Desulfovibrio africanus* (*Da*). The structure without bound substrate, as well as a complex with pyruvate and that of a reaction intermediate, have been solved (Chabriere et al., 1999; Chabriere et al., 2001).

Here, we report the structure of a PFOR enzyme isolated from a closely related species, *Desulfovibrio vulgaris* Hildenborough (*Dv*H). We show that the enzyme, which purifies as a 1056 kDa oligomer, exists as a stable tetramer of dimers, and we propose that a single residue insertion plays a significant role in this unusual oligomerization state. Our work demonstrates how extremely powerful negative stain electron microscopy can be in the context of proteomic comparisons between related microbes, or between different physiological states of a single microbe, when there is already at least one homolog X-ray structure and the genome for the new organism of interest available.

2. Materials and methods

2.1. Biomass production

Desulfovibrio vulgaris Hildenborough (ATCC 29579) was obtained from the American Type Culture Collection (Manassas, VA). A defined lactate–sulfate medium, LS4D, is used in all cultures. All media preparation details and reagents are as before (Mukhopadhyay et al., 2006). All reagents and preparation protocols are tracked for each media preparation and recorded in the Biofiles database (http://vimss.lbl.gov/perl/biofiles). Media are autoclaved and then filter sterilized, after which phosphate, vitamins and reducing agent (titanium citrate) are added. Stock cultures of *D. vulgaris* were prepared by growing the ATCC culture to log phase, and storing at −80 °C. The starter culture is prepared inside an anaerobic chamber using stock culture at a ratio of 1 ml stock/100 ml LS4D. The starter culture is incubated at 30 °C and allowed to grow for 48 h to log phase (optical density at 600 nm of ~0.3–0.4; $\sim 3 \times 10^8$ cells/ml). From the starter culture, a 10% subculture for inoculating the production culture is made in LS4D, in the anaerobic chamber, and incubated at 30 °C until log phase growth is reached (around 15 h). The generation time for *D. vulgaris* on this medium is 5 h. To minimize repetitive culturing "phenotypic drift" all experiments are started from fresh frozen stock. All experiments were run on cells that are less then three subcultures from the original ATCC culture. All inoculations and transfers were done in a Coy anaerobic glove box chamber (Coy Laboratory Products Inc., Grass Lake, MI) with an atmosphere of 5% CO_2, 5% H_2 and 90% N_2. The production culture is grown in batch, using a 5 L flask. The flask is autoclaved with 5 L LS4D media and cooled on the bench in the anaerobic chamber. Immediately before inoculation, vitamins, phosphate, and reducing agent are injected into the flask. Samples are periodically taken from the fermenter to monitor growth from OD measurement. Once log phase growth is reached, the cells are harvested. To minimize sample variability due to processing time, samples were pulled from the production cultures by peristaltic pump through 7 m of capillary tubing in an ice bath. This was found to drop the temperature of the sample to less then 4 °C in less then 15 s. The samples are directly put into 500 mL centrifuge bottles, which are centrifuged at 6000*g* for 10 min, with refrigeration at 4 °C (Beckman Coulter, Avanti J-25). The supernatant is discarded; the pellets are washed with degassed phosphate buffered saline solution, and pooled for a second spin. The bottles are flash-frozen in liquid nitrogen and stored at −80 °C until further processing.

2.2. Purification and biochemical characterization of PFOR

Cell extracts were produced by thawing 10 g of pelleted cells in 10 ml of 0.1 M Tris–HCl pH 7.5 containing 80 mM KCl, 2 mM dithiothreitol (DTT), 1 mM phenylmethylsulphonylfluoride (PMSF). Cells were broken by treatment with 0.5 mg/ml lysozyme for 2 h followed by sonication. The cytosolic portion of the cell extract was separated by centrifugation at 200,000*g* for 90 min and the supernatant was retained for purification of PFOR (Yu et al., 2001). All purification steps were performed at 4 °C using columns and an AKTA FPLC from GE Healthcare. Different mixtures of two buffers were used for column fractionation: Buffer A contained 25 mM Hepes pH 7.6, 10% (v/v) glycerol, 2 mM DTT, 0.01% (v/v) NP 40 and Buffer B contained Buffer A plus 1 M NaCl. The NaCl concentration of the mixture of the two buffers is given by the % Buffer B.

The cell extract supernatant was loaded on a 1.6 × 20 cm Q Sepharose Fast Flow column equilibrated with 5% buffer B. After the column had been washed with two column volumes of equilibration buffer, the bound proteins were eluted with 50% buffer B. All fractions containing significant amounts of protein were pooled and buffer exchanged to 5% buffer B with a 2.6 × 20 cm G-25 desalting column. The eluate was loaded to a 1.6 × 10 cm MonoQ column equilibrated with 5% buffer B. Then the MonoQ column was developed with a linear gradient from 5% buffer B to 50% buffer B in 25 column volumes and 4 ml fractions were collected. The fractions subsequently determined to contain PFOR were pooled and loaded onto a 1.6 × 60 cm Superdex 200 column equilibrated with 5% buffer B. Fractions eluted from that column in 5% buffer B were frozen in liquid nitrogen and stored at −70 °C. Purified Superdex 200 fractions were buffer exchanged using a PD-10 desalting column equilibrated with 10 mM Hepes, pH 7.6, 2 mM DTT, 0.01% NP40. The buffer-exchanged protein was concentrated with Amicon and Microcon centrifugal filters (Millipore) to a concentration of 0.2–0.6 mg/ml. The protein concentration was then determined with Coomassie Plus Bradford Assay Reagent (Pierce) using BSA as the standard.

The molecular weight of purified protein complexes was determined independently using native 4–20% PAGE (Bio-Rad) and gel filtration on a 1×30 cm Superose 6 column equilibrated with 5% Buffer B. The molecular weight standards used to calibrate the Superose 6 column were BSA (67 kDa), aldolase (158 kDa), catalase (223 kDa), ferritin (440 kDa), and thyroglobin (663 kDa). The Kav at which the *Dv*H PFOR complex eluted from the column was 0.30, suggesting an apparent molecular mass of 1000 kDa from the calibration curve. The apparent molecular weight of the monomer subunit was determined by 4–20% SDS–PAGE (Bio-Rad).

The identity of the 130 kDa polypeptide observed in SDS–PAGE was determined by in-gel digestion of a gel slice containing this polypeptide according to an established protocol (Jiménez et al, 2006). Modified porcine trypsin from Promega was used at a final concentration of 12.5 ng/ml in the digestion. Mixtures of proteolytic peptides were analyzed by nanoLC MS/MS utilizing an Ultimate Capillary LC System (Dionex) interfaced with QStar XL mass spectrometer (Applied Biosystems/Sciex) equipped with a Protana nanospray source. External calibration was performed in MS/MS mode using fragment ions of Glu-fibrinopeptide.

LC Packings Pepmap C18 trap column (300 μm inner diameter, 5 mm length, 300 Å pore size, 5 μm bead size) and a column (75 μm inner diameter, 15 cm length) self-packed with Jupiter Proteo C12 end-capped material (90 Å pore size, 4 μm bead size) were used for desalting and reversed phase peptide separation, respectively. A 50 min linear gradient from 2% B to 50% B was run at 250 nL/min flow rate, utilizing solvents A: 2% acetonitrile/0.1% formic acid and B: 80% acetonitrile/0.08% formic acid. Precursor ion selection employed an automated routine (Information Dependent Acquisition, IDA, Analyst QS 1.1. Applied Biosystems/Sciex) that consisted of a series of one survey MS scan (1 s, m/z 400–1700) and two MS/MS scans (2 s, m/z 60–1500); nitrogen served as a collision gas and collision energy was automatically adjusted depending on the size and charge state ($/m/z/$) of the precursor ion. In-house Mascot search engine version 2.1.01 (Matrix Science) was employed utilizing the following settings: all species within NCBInr 20060905 (3946334 sequences; 1357962904 residues); precursor mass tolerance 100 ppm; fragment mass tolerance 0.1 kDa; tryptic digestion with 2 missed cleavages, fixed modifications: S-carboxyamidomethyl, variable modifications: deamidation (Asn and Gln); Met-sulfoxide; Pyro-Glu (from N-terminal Gln). With the settings described above and a confidence level at $p < 0.05$, ion scores higher than 52 indicated extensive homology or identity.

The Mascot search engine matched 106 MS/MS spectra representing 64 unique tryptic peptide sequences to PFOR (gi|46450850; DVU 3025) with an overall score of 2600. Ninety five of the matches ranked #1, out of which 18 achieved a high confidence score ($p < 0.05$). The overall sequence coverage was 65%. Tryptic peptide ^{383}VNGP^{387}K that encompasses 383 Val falls outside the mass range of MS analysis and was not detected. Peptides containing amino acid residues Pro267, Pro318 and Ala319 were detected. In addition, a putative pyruvate carboxylase (gi|46449660; DVU 1834) was also identified as a potential hit with the overall score of 70 and sequence coverage of 5%. For this protein, 6 MS/MS spectra matches represented 6 unique tryptic peptide sequences, 3 matches ranked #1 and none achieved a high confidence score. We assume that this putative carboxylase is a minor contaminant of the PFOR preparation.

2.3. Electron microscopy of negatively stained samples

The PFOR sample was diluted with 1% trehalose from an initial concentration of 0.3 mg/ml to a concentration of 0.05 mg/ml. Three microliter of this sample was adsorbed onto a glow-discharge treated, carbon-coated grid for 30 s. The grid was first washed by touching a drop of 1% trehalose with the sample facing down for 10 s. The grid was then transferred to a solution containing 5% ammonium molybdate (pH 7) and 1% trehalose and stained for 30 s. The excess stain was blotted with filter paper and air-dried.

Data were collected on a Tecnai 12 (FEI Company) microscope operated at 120 keV on Kodak SO-163 film under low-dose conditions at a magnification of 49,700× with a defocus ranging from −0.6 μm to −1.6 μm. Micrographs were digitized in a Nikon Super Coolscan 8000 with scanning resolutions of 12.7 μm/pixel, resulting in resolutions of 2.56 Å/pixel at the level of the sample.

2.4. Cryo-EM

Cryo-EM samples were prepared on holey quantifoil grids (Quantifoil Micro Tools, GmbH), either with or without an additional thin layer of continuous carbon. In the first case (sample on continuous carbon), a 1.2 mg/ml PFOR sample was diluted to a concentration of 0.5 mg/ml. In the second case (sample over holey carbon) we used the undiluted sample, with a small amount of TMV added as an internal standard for size and image quality. In both cases, 3 μL of the protein samples were applied to a freshly glow-discharged grid mounted in a Vitrobot chamber set at 95% relative humidity and 23 °C. The grids were blotted for 2 s and immediately plunge-frozen in liquid ethane in order to vitrify the sample. Images were taken on a Tecnai 20 (FEI Company) microscope operated at 200 keV on Kodak SO-163 film under low-dose conditions at a magnification of 50,000 times.

2.5. Data processing of particles imaged in negative stain

Two steps were used for the overall reconstruction process:

For the first step, 10,411 particles were selected manually from 19 micrographs and windowed out using

EMAN's Boxer with a box size of 160×160 pixels (Ludtke et al., 1999). The boxed images were corrected for the CTF by phase flipping using ctfit (EMAN) and grouped into 80 classes by reference free classification using the EMAN commands ctfit and startnrclass, respectively. A set of Euler angles was then assigned to 20 of these class averages and an initial 3-D model was built by using common lines in Fourier space with the EMAN startAny command, assuming D4 symmetry of the complex. This model was low pass filtered to 50 Å resolution and taken as a preliminary model for 12 iterations of refinement using EMAN's refine command. A resolution of 21 Å of the final volume was determined by calculating the Fourier shell correlation between two volumes which had been built independently by splitting the dataset into two halves (EMAN's eotest). These volumes were also visually compared to a 21 Å low passed filtered volume of the X-ray structure 1B0P (Chabriere et al., 1999) of the PFOR homodimer from *Desulfovibrio africanus*. A good overall correspondence could be seen between the dimer volume and a quarter of the refined volume, confirming that the reconstruction had converged to the correct model.

For the second step, 14,496 particles were semiautomatically selected from the same micrographs mentioned above using 40 2-D projections of the previously determined model as a reference (using EMAN's *makeboxref.py* script and Boxer). The selected particles were grouped in 5 defocus groups and aligned to 83 2-D projections of the previous model using SPIDER's AP_SH command (the 2-D projections were modified by the Contrast Transfer Function, using the mean defocus value of each corresponding defocus group) (Frank et al., 1996). Fifteen percent of the particles with the lowest cross-correlation value were removed from each defocus group and the remaining 12,402 particles were used for a refinement with SPIDER. A resolution of 17 Å was reached by imposing D4 symmetry (using BP_32F) and 21 Å without imposing symmetry (using BP_CG).

EMAN v1.7 and SPIDER 13 (in combination with SPIRE) were the software versions used for reconstruction. All the resolutions reported correspond to the 0.5 FSC criterions.

2.6. Building a three-dimensional PFOR DvH model

A three-dimensional homology model of PFOR dimer from *Dv*H was produced using Modeller 8v2, which creates models based on the satisfaction of spatial restraints (Sali and Blundell, 1993). The sequence of the target protein was aligned to the *Desulfovibrio africanus* PFOR sequence using the program MUSCLE (Edgar, 2004) and the known X-ray structure 2C3M (Cavazza et al., 2006) was used as a template for the determination of the tertiary structure. The homology PFOR dimer model was docked (rigid-body fitting) into the PFOR octomer electron density using the program colors from the program package Situs 2.2 (Chacon and Wriggers, 2002).

The reconstructed densities presented here were normalized using the EMAN program proc3d (mean = 0, sigma = 1) and rendered with a threshold level of 1.9. This threshold was chosen to correspond to a volume that included almost all backbone atoms of the fitted homology model, allowing only small segments of loops to stick out of the volume. The size of the volume was measured with chimera (Pettersen et al., 2004) to be 2.05×10^6 A^3. The expected size of a 1.06 MDa protein (PFOR octomer) is 1.30×10^6 A^3 assuming a protein density of 1.35 g/cm^3. Therefore, the scaling factor between the expected and measured volume based on our study is 1.6. This scaling factor should be generally applicable to other studies, even though the current work used ammonium molybdate in combination with trehalose as a negative stain. The remarkable fit of an atomic model into the surface contours of our reconstruction, as demonstrated by the subsequent docking, should make this work a valuable point of reference to establish the appropriate isosurface level to be used in the interpretation of maps.

A model of the electrostatic potential (in water) of one of the fitted homology dimers was calculated using Delphi (Rocchia et al., 2001) and projected onto the *Dv*H PFOR octomer isosurface using the Chimera package from the Resource for Biocomputing, Visualization, and Informatics at the University of California, San Francisco (supported by NIH P41 RR-01081) (Pettersen et al., 2004).

3. Results

3.1. Purification of *DvH* PFOR

As part of an interdisciplinary project that is developing high-throughput approaches to identify and characterize microbial multi-protein complexes (http://pcap.lbl.gov/), this enzyme was initially purified as an unknown protein complex to at least 90% homogeneity (Fig. 1a and b). Both native gradient PAGE and Superose 6 gel filtration chromatography indicated that the molecular mass of the complex was approximately 1000–1300 kDa (Fig. 1a and b and data not shown). In SDS–PAGE, only a single polypeptide of 130 kDa was apparent. Mass spectrometry analysis of a gel slice including this 130 kDa band identified the protein as the 1215 amino acid, 132,690 kDa PFOR polypeptide (gi|46450850; DVU 3025). Thus the complex is a *Dv*H PFOR that appears to form a higher order multimer than reported for the *Desulfovibrio africanus* protein or any other PFOR enzyme.

3.2. Electron microscopy and 3-D reconstruction

Electron micrographs of negatively stained *Dv*H PFOR reveal that the particles are homogeneous in size and uniformly distributed on the carbon film of the EM grid (Fig. 2a). About 15,000 particle projections were boxed and subjected to two-dimensional reference-free alignment and classification. As is seen in the examples shown in

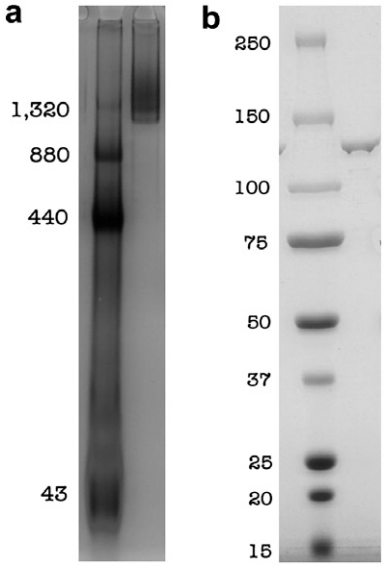

Fig. 1. Native PAGE and SDS–PAGE of the purified *Dv*H PFOR. (a) Native PAGE 4–15% (b) SDS–PAGE 4–20%. For each gel, the right lane contains purified PFOR and the left contains marker proteins whose molecular masses in kDa are indicated.

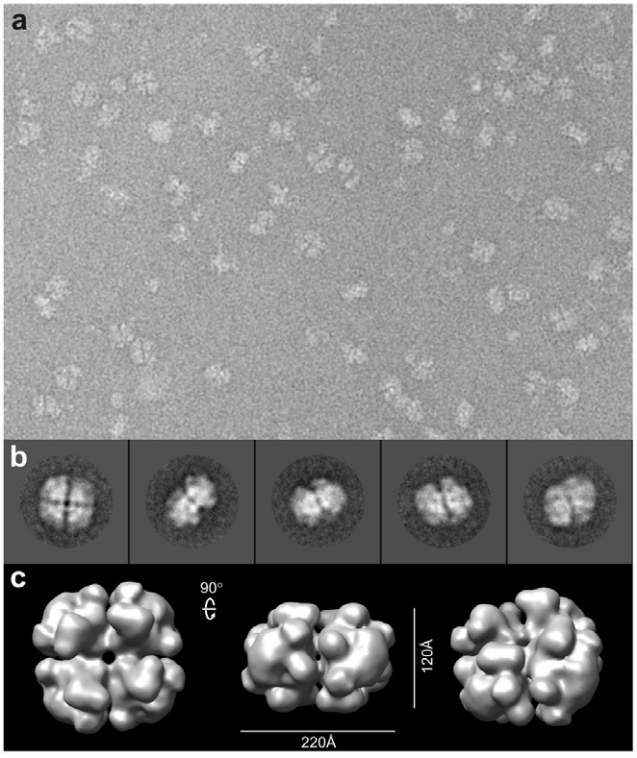

Fig. 2. Electron microscopy and 3-D reconstruction of *Dv*H PFOR. (a) Electron micrograph of the negatively stained sample. (b) Examples of reference-free two-dimensional class averages showing a "top view", two "side views" and two "tilted views" from left to right. Image averages reveal 4-fold and 2-fold symmetries in the top view and the side view representation, respectively. (c) Isosurface representation of the 17 Å resolution reconstruction from different views.

Fig. 2b, some class averages exhibited clear 4-fold symmetry, while some others exhibited 2-fold symmetry. In the following description, these symmetrical views will be referred to as the "top view" and "side views", respectively.

A Fourier common-lines routine was utilized to determine the relative orientations of 20 selected class averages, which were then combined to generate an initial 3-D model using EMAN (Ludtke et al., 1999). This initial model was used as a starting reference for projection-matching refinement in SPIDER (Frank et al., 1996), which resulted in a final model at 17 Å resolution after imposing D4 symmetry (Fig. 2c) and 21 Å without imposing symmetry (Fig. 3a). As is seen in Fig. 3b, the angular distribution of the particles that were used for the 3-D reconstruction shows a relatively even coverage, but with a clear preference for large and small θ angle corresponding to the top and side views, respectively.

The reconstruction reveals that PFOR, isolated from *Dv*H, is an octomer with a diameter of 200 Å and a height of 120 Å, consistent with the size and molecular weight estimated during biochemical purification. As mentioned before, there is only one PFOR crystal structure, that for the enzyme from *Desulfovibrio africanus.* A comparison between the *Dv*H and *Da* PFOR sequences, shown in Fig. 4, reveals an identity of 69%. Due to this high homology and the fact that the *Da* PFOR is a homo-dimer, one can expect that the *Dv*H PFOR octomer is composed of four dimers with a high similarity to the X-ray crystal structure of *Da* PFOR. This expectation was checked by docking the *Da* PFOR dimer structure into our *Dv*H PFOR EM density map via rigid-body fitting using the program colores from Situs 2.2 (Chacon and Wriggers, 2002). As is shown in Fig. 5a, there is an excellent match between the surface corrugations, or apparent domains, of the EM density and the corresponding features of the X-ray crystal structure. Docking of the dimer structure into the EM density map thus confirms that there is a high structural identity between these two homologs, as expected.

A closer look at the sequence comparison reveals that the *Da* PFOR sequence includes 13-residues at the C-terminal end that are absent in the *DvH* PFOR sequence. These residues form a short α-helix in the *Da* crystal structure that is clearly outside of the envelope of the *Dv*H PFOR EM-reconstruction (Fig. 5a). The fact that this 1.5 kDa short helix of the *Da* structure sticks out of the *Dv*H density map serves as an internal demonstration of the remarkable accuracy of the surface features within an EM density map of a negatively stained specimen at a resolution of 17 Å.

3.3. Homology model and the basis of oligomerization

The high sequence homology that exists between *Da* PFOR and *Dv*H PFOR makes it possible to create a reasonable homology model of the *Dv*H PFOR octomer. We thus built a homology model for the *Dv*H PFOR dimer

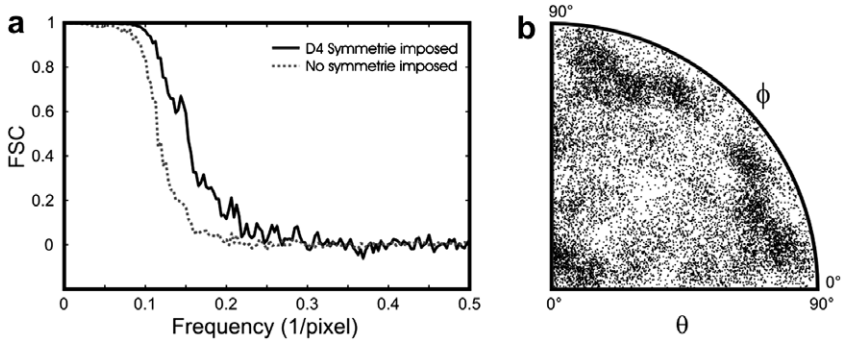

Fig. 3. Fourier shell correlation and angular distribution for the *Dv*H PFOR reconstruction. (a) Comparison of separate reconstructions from two halves of the data shows a resolution of 17 Å and 21 Å at 0.5 FSC, with and without imposing D4 symmetry during refinement, respectively. (b) Angular distribution of all particles in the data set. Due to the symmetry, just the absolute angle values are shown. The coverage of angular space is fairly even and thus the resolution of the volume is expected to be isotropic.

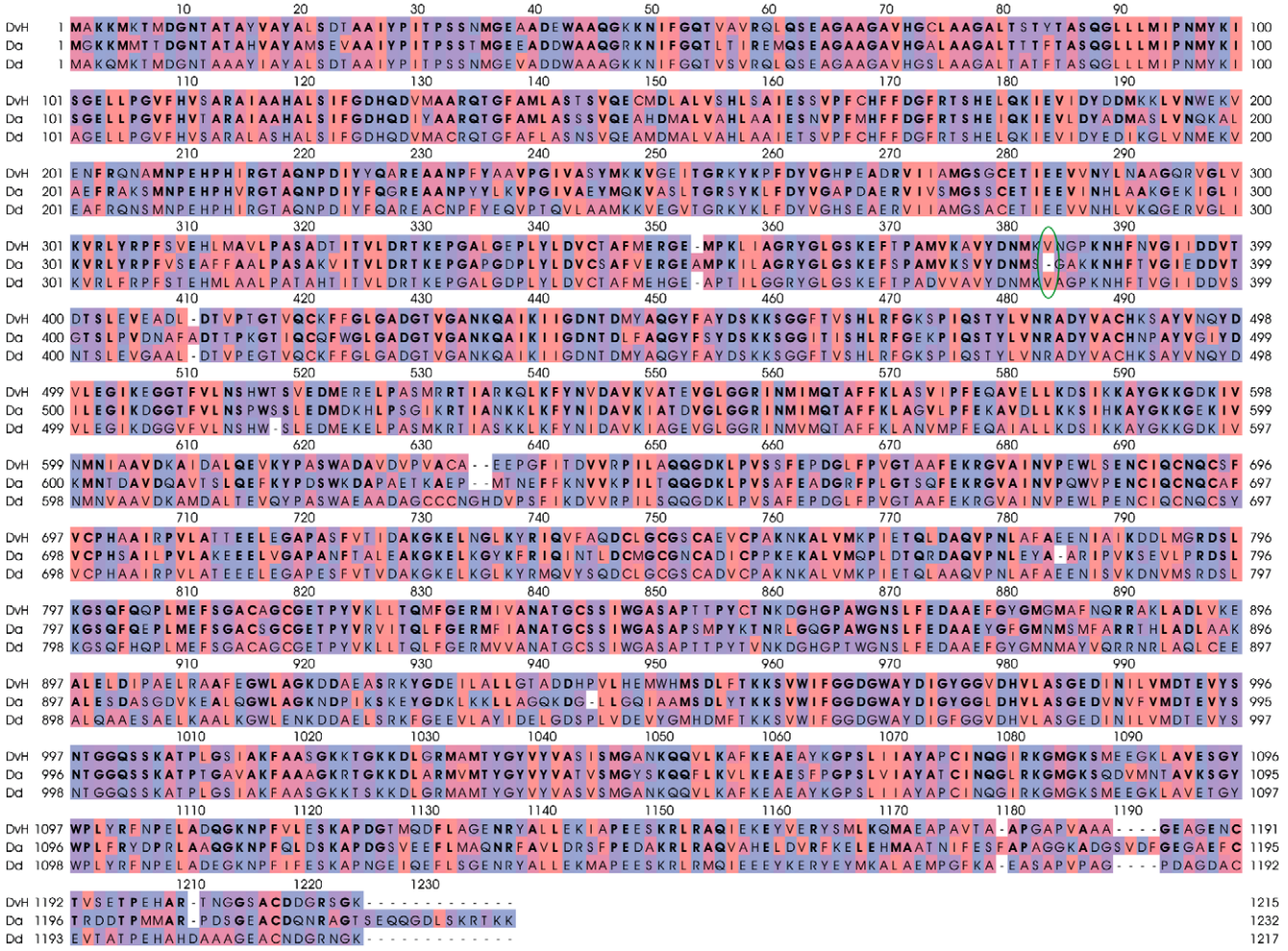

Fig. 4. Sequence alignment of PFOR from *Desulfovibrio vulgaris (Dv*H), *Desulfovibrio africanus (Da)* and *Desulfovibrio desulfuricans (Dd)*. Sequences were aligned using Muscle. Hydrophobic residues are shown in red and hydrophilic in blue. The Val383 insertion is circled and highlighted in green. Identical residues in *Dv*H and *Da* are highlighted in bold.

using the *Da* PFOR X-ray structure and the *Dv*H PFOR sequence using 2C3M (Cavazza et al., 2006). This dimer model was then docked (using colores) into the EM density in order to produce the final homology model of the PFOR octomer shown in Fig. 5b and c. The accuracy of the docking is shown in Fig. 5d, where the value of the cross-correlation scoring function is plotted as a function of the two translational variables X and Y in the plane of maximal correlation for Z and at maximal correlation of each Euler angle. The identity of the four correlation peaks is, of

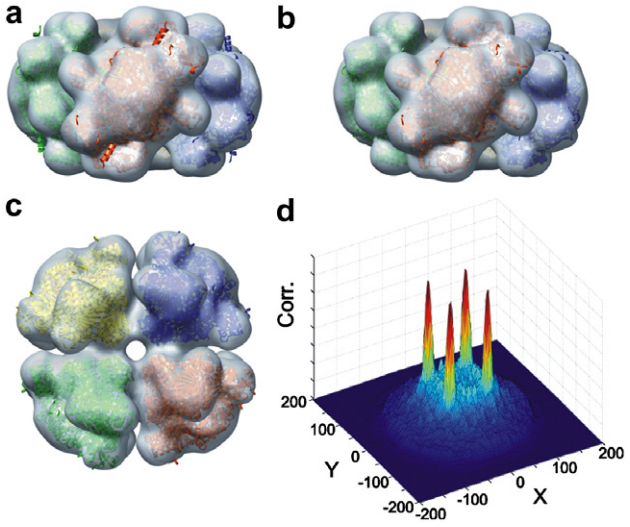

Fig. 5. Docking atomic models into the *Dv*H PFOR EM density by an exhaustive 6D rigid-body search (Chacon and Wriggers, 2002) (a) *Desulfovibrio africanus* (*Da*) PFOR dimer X-ray structure docked into the *Dv*H PFOR map at four different positions (shown in four different colors). (b) as (a), but for a homology model of the *Dv*H PFOR dimer. (c) Another view of the structure in (b). (d) Laplacian correlation value as a function of the two translation variables X and Y in the plane of maximal correlation for Z and at maximal correlation of each Euler angle ($\mathrm{corr}(Z,\theta,\varphi,\psi) = \max$).

course, a consequence of the fact that D4 symmetry was imposed when computing the 3-D density map. The height and sharpness of the cross correlation curve nevertheless shows that the correct position for docking the homology model into the EM density map is completely unambiguous.

To reveal the chemical basis for the oligomerization of *Dv*H PFOR, we next looked more closely at the interface between two adjacent dimers in the octomer. As is shown in Fig. 6, the point of closest contact between dimers is occupied by a valine residue (Val383, blue) that is "inserted" into a surface loop of the *Dv*H primary structure but is absent in the primary structure of *Da* PFOR. The immediate neighbors of this hydrophobic residue in the adjacent dimer are three nonpolar residues: Pro267 (red), Pro318 (yellow) and Ala319 (orange). Unlike Val383, these residues are also present in the *Da* PFOR sequence.

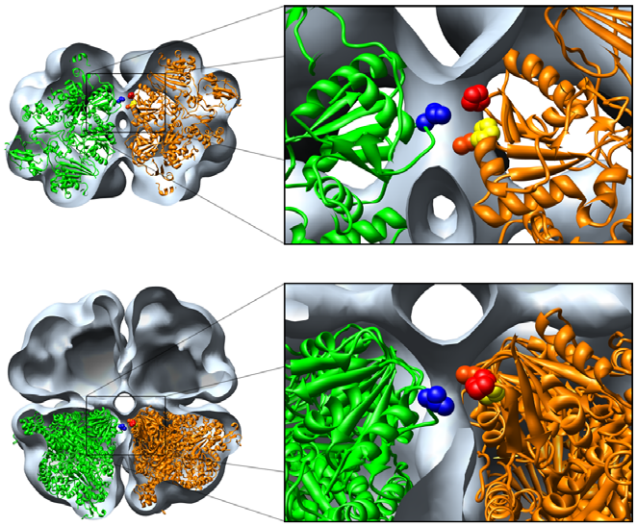

Fig. 6. Interaction between two *Dv*H PFOR dimers. Side and top view of the *Dv*H PFOR isosurface cropped at the position of closest contact between adjacent dimers. The interaction region is occupied by Val383 (blue), Pro267 (red), Pro318 (yellow) and Ala319 (orange).

3.4. Cryo-EM attempts and octomer stability

The previous analysis indicates that the *Dv*H PFOR dimers assemble into octomers using a minimal number of hydrophobic interactions. Interestingly, an anomalous behavior of the complex was observed when attempting cryo-EM studies. When samples where prepared on holey carbon films and visualized through holes, the complexes appeared to have broken down into dimers or even smaller species (Fig. 7a). However octomers appeared intact when

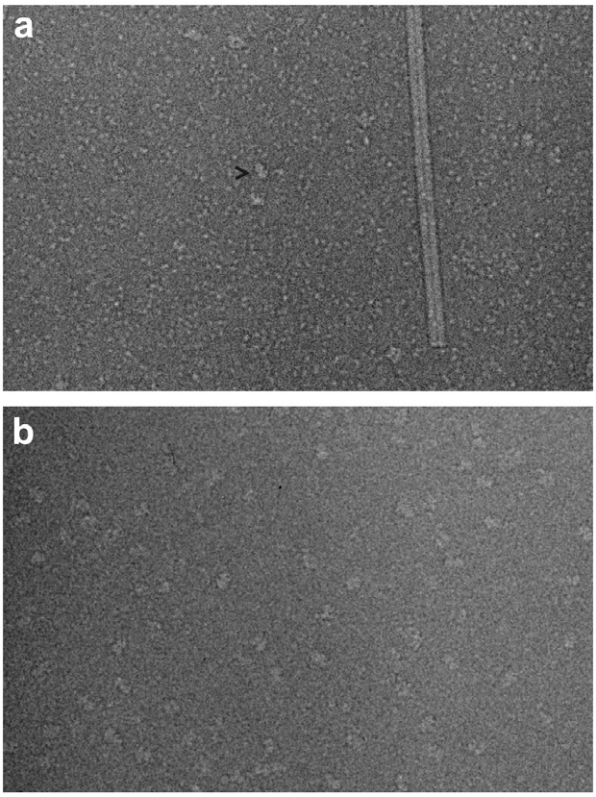

Fig. 7. Electron micrographs of vitrified PFOR. (a) Protein concentration: 1.1 mg/ml. Sample preparation over holey carbon with Tobacco Mosaic Viruses (TMV) as an internal standard (defocus −7 μm). The black arrow points to an undisrupted *Dv*H PFOR octomer showing the protein in a "side view". One TMV virus can be seen as a long rod on the right side of the image. The diameter of TMV is about 180 Å and therefore comparable to the diameter of a PFOR octomer. It is clear that the majority of the protein has dissociated into smaller particles that we believe to be PFOR dimers. These smaller particles are not present on micrographs of negatively stained samples (see Fig. 3a). (b) Specimen absorbed to continuous carbon (defocus –5 μm). Protein concentration: 0.5 mg/ml. The size and shape of the particles correspond to octomeric *Dv*H PFOR.

samples were prepared on a continuous carbon film (Fig. 7b). When PFOR octomers were crosslinked with gluteraldehyde they remained intact, even when prepared on holey carbon (data not shown).

Sample preparation over holes contains a step where the protein is confined for a brief period of time (before it gets vitrified) between two closely apposed, fresh air–water interfaces. Since the thickness of the water layer is, in the ideal case, not much greater than the size of the protein itself, a freely mobile protein can collide multiple times with the water/air interface. In the worst case, adsorption to the air–water interface will denature the protein (Dickinson, 1999). In the case of *Dv*H PFOR it seems that the hydrophobic residues which are responsible for assembly of the octomer also have a high affinity for the air interface.

It is reasonable that the disassembly of the complex can be avoided, to a large extent, by immobilizing the protein on a hydrophilic surface. The rationale is that binding of a protein via electrostatic forces on a freshly glow discharged carbon film (Dubochet et al., 1982) restrains the particle from colliding with a fresh air–water interface shortly after blotting the sample. The preparation of ice-embedded samples on continuous carbon has some disadvantages, however, one of which is that the carbon film adds noise to the images and another being the possibility of preferential orientation of particles. Fortunately, the symmetry present in the *Dv*H PFOR complex allows processing with higher noise level, and the particles seem to adopt multiple orientations on the carbon support (as demonstrated by our negative stain studies), likely due to the presence of multiple patches of positive charge on its surface that have the potential to allow for multiple adsorption orientations.

4. Discussion

Our study shows that pyruvate-ferredoxin oxidoreductase from *Desulfovibrio vulgaris* Hildenborough is a homo-octomer with a molecular weight of about 1 MDa. Two monomers of this enzyme assemble into a dimer in a very similar manner to that observed for the closely related species *Desulfovibrio africanus.* While PFOR remains a dimer in *Da*, the *Dv*H PFOR dimers further oligomerize into a higher-symmetry complex. The increased size as well as the D4-symmetry makes this complex ideal for characterization by electron microscopy and single particle reconstruction.

The overall structure of the PFOR octomer that is deduced from 3-D electron microscopy of negatively stained samples shows that the surface contour of the protein is well preserved by using an ammonium molybdate, trehalose mixture as a negative stain. The accurate docking and the tight match of the homology model and the EM map indicate that no significant molecular flattening or disorder of exposed domains occurs during specimen preparation. This is most likely because the collapse of the specimen due to dehydration was prevented by the stabilizing and protecting properties of trehalose (Harris et al., 1996), although the globular character of the monomer and its tight D4 packing in the octomer may also play a role in the mechanical robustness of the complex. The remarkable sensitivity and accuracy of the surface contour in our reconstruction is fully appreciated after docking the *Da* PFOR structure into the *Dv*H EM map. The additional short C-terminal α-helix that is present in *Da* PFOR clearly sticks out of the volume in Fig. 5a, indicating that this helix is absent in *Dv*H PFOR, as corroborated by the gene-sequence information.

A realistic three-dimensional model of the *Dv*H PFOR octomer was obtained by combining homology modeling and structural docking. The resulting *Dv*H PFOR octomer model clearly shows that a valine residue, which is inserted into a surface loop of the *Dv*H PFOR, sits precisely at the point of closest contact between adjacent dimers in the octomer in an area of high protein density. It should be noted that the actual conformations of the displayed side chains cannot be known from computational modeling based on docking a homology structure into an EM structure at this resolution (17 Å). Nevertheless, it can be assumed that at least the peptide backbone positions are reasonably accurate due to the high homology between the two proteins and the precise docking. Therefore one can be confident that the insertion of Val383 into a *Dv*H PFOR surface loop plays a significant role in formation of an octomeric complex, doing so through a hydrophobic interaction with Ala319.

Beside this insertion, other replacements of hydrophilic amino acids with hydrophobic ones can be noted within the sequence that is shown in Fig. 4. None of these substitutions are found in the vicinity of the dimer–dimer interaction sites, however. Thus, the insertion of a single valine residue might be exclusively responsible for the formation of a PFOR octomer in *Dv*H. The valine insertion found in the *Dv*H PFOR sequence is also found in PFOR from *Desulfovibrio desulfuricans* (*Dd*) at exactly the same position (Fig. 4). The quaternary structure of *Dd* PFOR is not known yet, but it can now be predicted that it would correspond to the homo-octomeric structure of *Dv*H PFOR.

In order for the *Dv*H PFOR to perform its enzymatic reaction, it is crucial that the binding site for ferredoxin is not sterically occluded when the dimers are assembled into the octomeric complex. Once the homology model was built, therefore, we asked whether the ferredoxin binding site in the proposed structure of the octomer was still fully exposed to solvent. Fig. 8 shows the surface of the PFOR octomer, colored according to the electrostatic potential of the homology dimer. Blue represents positive potential, red negative, and zero potential is white. On the basis of NMR restrained docking it has been proposed that ferredoxin binds to the *Da* PFOR dimer at a position close to the distal [4Fe–4S] cluster (Pieulle et al., 2004). The binding sites of the negatively charged ferredoxin molecule are expected to be dominated by electrostatic forces, i.e. by

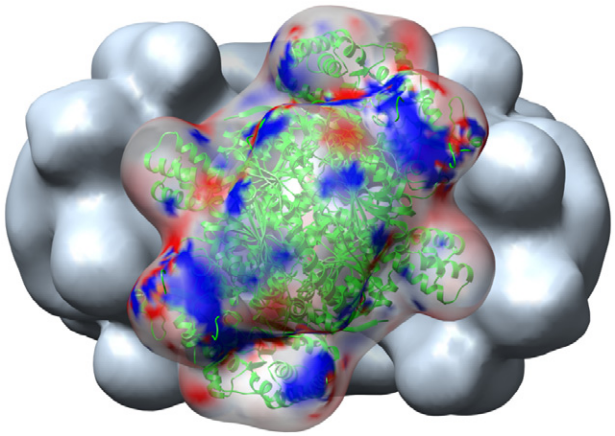

Fig. 8. Electrostatic contour surface of one *Dv*H PFOR. Blue represents positive potential, red negative and the potential around zero is white. The largest positively charged area is also the proposed ferredoxin binding site (Pieulle et al., 2004).

a region of positive electrostatic potential on the surface of PFOR. The ferredoxin binding site that was proposed on these grounds by Pieulle et al. corresponds with the two largest blue areas in the upper right and lower left side of the represented dimer. This image therefore reveals that the proposed ferredoxin binding site is still located on the fully exposed surface of the octomer, i.e. it is not blocked after oligomerization of the dimers into an octomer.

Sickle-cell hemoglobin is a well-known example in which a single point mutation leads to the oligomerization of smaller protein units (Ingram, 1957). The substitution of Glu6 by valine in the two β-chains of wild-type hemoglobin leads to the assembly of long, multistranded bundles of deoxyhemoglobin, which in turn causes major structural changes of red blood cells and hinders their passage through the microcirculation.

While the valine mutation that leads to the formation of higher oligomers of hemoglobin causes a human disease, the formation of PFOR octomers in *Dv*H must be in some way advantageous to the biochemical physiology of this microorganism. This much can be deduced from the fact that this insertion is stable in the wild-type *vulgaris* genome.

At least four alternatives, all of which still remain to be characterized experimentally, can be suggested as reasons why the formation of an octomer is favored in *Dv*H. Perhaps the first suggestion to mention is that the formation of higher oligomers might increase the degree of cooperativity of catalysis. A second possibility is that subtle changes in tertiary structure that occur upon docking of dimers might lead to a conformational strain on the iron-sulfur redox centers of the enzyme, thereby "tuning" the redox potential in a way that is beneficial to the physiology of this particular microbe. More speculatively, a third possibility is that the formation of larger oligomers might affect the spatial and temporal performance of the metabolic network to which the enzyme contributes by altering the number of active catalytic centers that are co-localized at a given point within the cell. A fourth possibility is that the rate at which productive collisions occur between PFOR and ferredoxin might be increased because of the fact that oligomerization increases the ratio of active to inactive surface; in other words, inactive surfaces of the dimer are hidden within the interior of the octomer.

Acknowledgments

We thank Sacha De Carlo for help and suggestions with image analysis, Steven J. Ludtke for help with EMAN and Patricia Grob, Hong-Wei Wang, Bunpote Siridechadilok and Slaton Lipscomb for technical support with electron microscopy and image analysis. We are grateful to Scott Dixon for excellent technical assistance and to Steven Hall and Susan Fisher for their input on all aspects of mass spectrometry analysis. This research was supported in part by the Director, Office of Science, Office of Biological and Environmental Research, Genomics:GTL program of the US Department of Energy under Contract DE-AC02-05CH11231. The UCSF Biomolecular Resource Center Mass Spectrometry Facility acknowledges support from the Sandler Family Foundation. The award of a Feodor Lynen Fellowship from the Alexander von Humboldt-Foundation to FG is gratefully acknowledged. Eva Nogales is a Howard Hughes Medical Institute Investigator.

The density map reported here for PFOR has been deposited in the Macromolecular Structure Database (EBI) where it has been assigned the accession code EMD-1319.

Appendix A. Supplementary data

Supplementary data associated with this article can be found, in the online version, at doi:10.1016/j.jsb.2007.01.020.

References

Brostedt, E., Nordlund, S., 1991. Purification and partial characterization of a pyruvate oxidoreductase from the photosynthetic bacterium *Rhodospirillum rubrum* grown under nitrogen-fixing conditions. Biochem. J. 279, 155–158.

Cavazza, C., Contreras-Martel, C., Pieulle, L., Chabriere, E., Hatchikian, E.C., Fontecilla-Camps, J.C., 2006. Flexibility of thiamine diphosphate revealed by kinetic crystallographic studies of the reaction of pyruvate-ferredoxin oxidoreductase with pyruvate. Structure 14, 217–224.

Chabriere, E., Charon, M.H., Volbeda, A., Pieulle, L., Hatchikian, E.C., Fontecilla-Camps, J.C., 1999. Crystal structures of the key anaerobic enzyme pyruvate:ferredoxin oxidoreductase, free and in complex with pyruvate. Nat. Struct. Biol. 6, 182–190.

Chabriere, E., Vernede, X., Guigliarelli, B., Charon, M.H., Hatchikian, E.C., Fontecilla-Camps, J.C., 2001. Crystal structure of the free radical intermediate of pyruvate:ferredoxin oxidoreductase. Science 294, 2559–2563.

Chacon, P., Wriggers, W., 2002. Multi-resolution contour-based fitting of macromolecular structures. J. Mol. Biol. 317, 375–384.

Charon, M.H., Volbeda, A., Chabriere, E., Pieulle, L., Fontecilla-Camps, J.C., 1999. Structure and electron transfer mechanism of pyruvate:ferredoxin oxidoreductase. Curr. Opin. Struct. Biol. 9, 663–669.

Dickinson, E., 1999. Adsorbed protein layers at fluid interfaces: interactions, structure and surface rheology. Colloids Surf. B: Biointerfaces 15, 161–176.

Dubochet, J., Groom, M., Mueller-Neuteboom, S., 1982. The mounting of macromolecules for electron microscopy with particular reference to surface phenomena and the treatment of support films by glow discharge. Adv. Opt. Electron Microsc. 8, 107–135.

Edgar, R.C., 2004. MUSCLE: a multiple sequence alignment method with reduced time and space complexity. BMC Bioinformatics 5, 113.

Frank, J., Radermacher, M., Penczek, P., Zhu, J., Li, Y., Ladjadj, M., Leith, A., 1996. SPIDER and WEB: processing and visualization of images in 3D electron microscopy and related fields. J. Struct. Biol. 116, 190–199.

Harris, J.R., Gerber, M., Gebauer, W., Wernicke, W., Markl, J., 1996. Negative stains containing trehalose: application to tubular and filamentous structures. J. Microsc. Soc. Am. 2, 43–52.

Ikeda, T., Ochiai, T., Morita, S., Nishiyama, A., Yamada, E., Arai, H., Ishii, M., Igarashi, Y., 2006. Anabolic five subunit-type pyruvate:ferredoxin oxidoreductase from *Hydrogenobacter thermphilus* TK-6. Biochem. Biophys. Res. Commun. 340, 76–82.

Ingram, V.M., 1957. Gene mutations in human hemoglobin: the chemical difference between normal and sickle cell hemoglobin. Nature 180, 326–328.

Jiménez, C.R., Huang, L., Qiu, Y., Burlingame, A.L., 2006. In-gel digestion of proteins for MALDI-MS fingerprint mapping. Curr. Prot. Prot. Sci., 16.4.2–16.4.4.

Kletzin, A., Adams, M.W., 1996. Molecular and phylogenetic characterization of pyruvate and 2-ketoisovalerate ferredoxin oxidoreductases from *Pyrococcus furiosus* and pyruvate ferredoxin oxidoreductase from *Thermotoga maritima*. J. Bacteriol. 178, 248–257.

Ludtke, S.J., Baldwin, P.R., Chiu, W., 1999. EMAN: semiautomated software for high-resolution single-particle reconstructions. J. Struct. Biol. 128, 82–97.

Mukhopadhyay, A., He, Z., Alm, E.J., Arkin, A.P., Baidoo, E.E., Borglin, S.C., Chen, W., Hazen, T.C., He, Q., Holman, H.Y., Huang, K., Huang, R., Joyner, D.C., Katz, N., Keller, M., Oeller, P., Redding, A., Sun, J., Wall, J., Wei, J., Yang, Z., Yen, H.C., Zhou, J., Keasling, J.D., 2006. Salt stress in *Desulfovibrio vulgaris* Hildenborough: an integrated genomics approach. J. Bacteriol. 188, 4068–4078.

Pettersen, E.F., Goddard, T.D., Huang, C.C., Couch, G.S., Greenblatt, D.M., Meng, E.C., Ferrin, T.E., 2004. UCSF Chimera: a visualization system for exploratory research and analysis. J. Comput. Chem. 25, 1605–1612.

Pieulle, L., Nouailler, M., Morelli, X., Cavazza, C., Gallice, P., Blanchet, S., Bianco, P., Guerlesquin, F., Hatchikian, E.C., 2004. Multiple orientations in a physiological complex: the pyruvate-ferredoxin oxidoreductase-ferredoxin system. Biochemistry 43, 15480–15493.

Rocchia, W.E., Alexov, E., Honig, B., 2001. Extending the applicability of the nonlinear Poisson–Boltzmann equation: multiple dielectric constants and multivalent ions. J. Phys. Chem. B 105, 6507–6514.

Sali, A., Blundell, T.L., 1993. Comparative protein modeling by satisfaction of spatial restraints. J. Mol. Biol. 234, 779–815.

Yu, L., Ishida, T., Ozawa, K., Akutsu, H., Horiike, K., 2001. Purification and characterization of homo- and hetero-dimeric acetate kinases from the sulfate-reducing bacterium *Desulfovibrio vulgaris*. J. Biochem. (Tokyo) 129, 411–421.